Available online at www.sciencedirect.com
ScienceDirect
Journal of Computational Physics 227 (2008) 2864–2885
JOURNAL OF COMPUTATIONAL PHYSICS
www.elsevier.com/locate/jcp

On solutions to the P_n equations for thermal radiative transfer

Ryan G. McClarren [a,*,1], James Paul Holloway [b], Thomas A. Brunner [c,2]

[a] *Computational Physics and Methods Group, Los Alamos National Laboratory, P.O. Box 1663, MS D413 Los Alamos, NM 87545, United States*
[b] *Department of Nuclear Engineering and Radiological Sciences, College of Engineering, University of Michigan, 2355 Bonisteel Boulevard, Ann Arbor, MI 48109 2104, United States*
[c] *Sandia National Laboratories, P.O. Box 5800, MS 1186, Albuquerque, NM 87185 1186, United States*

Received 7 May 2007; received in revised form 15 November 2007; accepted 19 November 2007
Available online 4 December 2007

Abstract

We present results for the spherical harmonics (P_n) method for solving problems of time-dependent thermal radiative transport. We prove a theorem that demonstrates that in the streaming limit, the spatially and temporally continuous P_n equations will allow negative energy densities for any finite order of n. We also develop an implicit numerical method for solving the P_n equations to explore the impact of the theorem. The numerical method uses a high-resolution Riemann solver to produce an upwinded discretization. We employ a quasi-linear approach to integrate the nonlinearites added to make the scheme non-oscillatory. We use the backward Euler method for time integration and treat the material interaction terms fully nonlinearly. Reflecting boundary conditions for the P_n equations are presented and we show how to implement this boundary condition using ghost cells. The implicit method was able to produce robust results to thermal transport problems in one and two dimensions. The numerical method is used to analyze the accuracy of various P_n expansion orders on several problems. In two-dimensional problems the numerical P_n solutions contained negative radiation energy densities as predicted by our theorem. The numerical results showed that the material temperature also became negative, a result outside the scope of the theorem. Our numerical method can handle these negative values, but they would cause problems in a radiation-hydrodynamics calculation.
Published by Elsevier Inc.

Keywords: Thermal radiation transport; P_n approximation; Nonlinear solver; Implicit time integration

1. Introduction

The numerical solution of the equations that govern the physics of thermal radiation transport is a difficult task due at least in part to the number of independent variables in the system and the nonlinear evolution of

* Corresponding author. Tel.: +1 505 665 1397.
E-mail address: ryanmc@lanl.gov (R.G. McClarren).

[1] Los Alamos National Laboratory is operated by Los Alamos National Security, LLC for the US Department of Energy under Contracts DE-AC52-06NA25396 and LA-UR-07-3011.

[2] Sandia is a multiprogram laboratory operated by Sandia Corporation, a Lockheed Martin Company for the United States Department of Energy's National Nuclear Security Administration under Contract DE-AC04-94AL85000.

0021-9991/$ - see front matter Published by Elsevier Inc.
doi:10.1016/j.jcp.2007.11.027

the material temperature. The field of deterministic transport of X-rays has mostly centered around discrete ordinates (S_n) and flux-limited diffusion (FLD) methods. The S_n method solves the transport equation along particular directions and uses a quadrature rule to determine the energy density at a given point. The solutions given by this method can have spatial oscillations in the energy density known as ray effects [1,2]. These effects are especially prominent when photons stream from a localized and isotropic source across an optically thin medium. In a simulation where the radiation transport is coupled to hydrodynamics of the background material these ray effects can lead to hot spots in the material and the material can consequently evolve incorrectly. FLD allows photons to non-physically diffuse around optically thick objects. In a radiation-hydrodynamics simulation this could also lead to the incorrect evolution of the system. For example if X-rays were shined on one face of a block of metal, FLD would allow the back of the block to be heated. This would make the radiative heating of the block more uniform that it would actually be.

Another deterministic method that could be applied to problems of radiative transfer is the spherical harmonics (P_n) method. This approach uses a truncated expansion of the angular variables to arrive at a finite hyperbolic system. In one dimension this method is equivalent to the S_n method using Gaussian quadrature; however, in multiple dimensions the two methods are different. P_n does not have ray effects in multiple dimensions, yet, the spatially and temporally continuous P_n equations can have negative energy density solutions in time-dependent problems. This unphysical result is a part of the reason the P_n method has been marginalized for thermal radiative transport.

Though it is well known that in time-dependent problems the P_n method can give negative solutions for the radiation energy density (see, for example, McClarren et al. [3] or Brunner and Holloway [4]), no study of the origin and behavior of the negative parts of the solution has been undertaken. In this study we present a theorem stating that the P_n equations can give negative results for any order of n except in slab geometry. The theorem hinges on the fact that the P_n equations are linear, hyperbolic, and rotationally invariant. We then develop a numerical scheme to show how the P_n equations behave in thermal radiative transfer problems. This allows us to explore how the magnitude of the negative parts of the solution behaves as the order of the expansion is changed. Moreover, we will explore how negative solutions for the radiation energy density impact the material temperature.

Discrete ordinates methods of solving the transport equation have the benefit of a rich body of research on their defects and on efficient solution techniques; their very success has contributed to the relative neglect of the P_n method. Of late there has been somewhat of a *risorgimento* of the P_n method for time-dependent problems. Brunner and Holloway developed robust methods for solving linear transport problems with spherical harmonics [4,5]. This work was based on the use of a high-resolution upwind method using explicit time integration. Their spatial discretization was a finite-volume Riemann solver using van Leer's limiter to achieve better than first-order accuracy. The success of this method goaded us to develop an implicit upwind scheme for P_n [6,7]. To have a high-resolution, implicit method it is necessary to solve a nonlinear system of equations at each time step. Using the minmod limiter, we were able to efficiently and accurately solve these nonlinear equations by a quasi-linear method that required solving two linear systems.

The numerical method in this paper is an extension of the quasi-linear implicit scheme [6] to thermal radiative transfer problems with a participating background medium. Our work represents the first use of an implicit Riemann method for thermal radiation transport. This scheme will be modified to solve the thermal transport system in a fully coupled manner. Using this scheme we are able to take time steps large compared to the radiation propagation time scale and on the order of the time scale of the material energy.

We will also show how to implement reflecting boundary conditions in a finite-volume P_n method. Previously, Brunner and Holloway explored different types of boundary conditions [5]. Of all the boundary conditions they examined, the Mark boundary condition implemented using ghost cells had the best combination of ease of implementation and accuracy. To use ghost cells, a cell is placed outside the physical system with the P_n moments specified. The Riemann solver appropriately moves only the incoming part of those moments into the system. We will use this type of implementation to specify a reflecting boundary.

We use our method to solve several problems in one and two dimensions. These problems range from simple problems with analytic solutions to 2D problems in complicated geometries. In one-dimensional problems P_n orders of seven or nine are able to capture many features of analytic transport solutions. The two-dimensional test problems support the results of our theorem by giving negative energy densities. The negative

energy densities persist even to high orders of n. These negative energy densities are worst at the interface of a dark region and an illuminated one. The negative radiation energy densities in these problems cause the material temperature to become negative as well.

2. Thermal radiative transfer P_n equations

The grey radiative transfer equation in the absence of scattering is [8]

$$\frac{1}{c}\frac{\partial I}{\partial t}+\widehat{\Omega}\cdot\nabla I=\sigma\left(\frac{1}{4\pi}acT^4-I\right)+\frac{Q}{4\pi}. \tag{1}$$

In this equation $I(\vec{x},\widehat{\Omega},t)$ is the radiation intensity, $\widehat{\Omega}$ is the angular variable, σ is opacity of the material with units (cm^{-1}); a is the radiation constant (1.372×10^{13} J m^{-3} keV^{-4}); c is the speed of light (3×10^{8} m s^{-1}); Q is a prescribed source that is angularly isotropic with units (J m^{-3} s^{-1}); T is the background material temperature in keV. We note that σ is a function of space, time and material temperature, however for convenience we do not explicitly write this dependence. The equation that governs the material temperature (assuming a stationary background material) is

$$C_v(T)\frac{\partial T}{\partial t}=\sigma\left(\int_{4\pi}I\,\mathrm{d}\widehat{\Omega}-acT^4\right), \tag{2}$$

with C_v the heat capacity of the material in units (J cm^{-3}/keV).

The P_n method writes the angular dependence of Eq. (1) as a series expansion in spherical harmonics functions. The P_n equations we use are an extension to thermal radiative transfer of 2D equations written by Brunner [4]. These equations are

$$\frac{1}{c}\frac{\partial I_l^m}{\partial t}+\frac{1}{2}\frac{\partial}{\partial x}\left(-C_{l-1}^{m-1}I_{l-1}^{m-1}+D_{l+1}^{m-1}I_{l+1}^{m-1}+\mathcal{E}_{l-1}^{m+1}I_{l-1}^{m+1}-F_{l+1}^{m+1}I_{l+1}^{m+1}\right)+\frac{\partial}{\partial z}\left(A_{l-1}^{m}I_{l-1}^{m}+B_{l+1}^{m}I_{l+1}^{m}\right)+\sigma I_l^m=0 \tag{3}$$

for $l\in[0,\infty)$ and $m\neq0$, $|m|\leqslant l$. The equation for I_1^0 is

$$\frac{1}{c}\frac{\partial I_1^0}{\partial t}+\frac{1}{2}\frac{\partial}{\partial x}\left(\mathcal{E}_{l-1}^{m+1}I_{l-1}^{1}-F_{l+1}^{m+1}I_{l+1}^{1}\right)+\frac{\partial}{\partial z}\left(A_{l-1}^{0}I_{l-1}^{0}+B_{l+1}^{0}I_{l+1}^{0}\right)+\sigma I_l^0=\frac{\sigma acT^4\delta_{l0}}{2\sqrt{\pi}}+\frac{Q\delta_{l0}}{2\sqrt{\pi}}. \tag{4}$$

The moments of the specific intensity, $I(x,z,\widehat{\Omega},t)$, are defined by

$$I_1^m(x,z,t)=\int_{4\pi}Y_1^{m*}(\widehat{\Omega})I(x,z,\widehat{\Omega},t)\,\mathrm{d}\widehat{\Omega}, \tag{5}$$

where the spherical harmonics functions are

$$Y_1^m(\widehat{\Omega})=\sqrt{\frac{2l+1}{4\pi}\frac{(l-m)!}{(l+m)!}}P_1^m(\cos\theta)\mathrm{e}^{\mathrm{i}m\varphi}, \tag{6}$$

with P_1^m an associated Legendre function. The zeroth moment of the intensity can be related to the radiation energy density by

$$E=\frac{1}{c}\int_{4\pi}I(x,z,\widehat{\Omega},t)\,\mathrm{d}\widehat{\Omega}=\frac{I_0^0}{2c\sqrt{\pi}}. \tag{7}$$

The constants in Eqs. (3) and (4) are

$$A_1^m=\sqrt{\frac{(l-m+1)(l+m+1)}{(2l+3)(2l+1)}},\quad B_1^m=\sqrt{\frac{(l-m)(l+m)}{(2l+1)(2l-1)}},$$

$$C_1^m=\sqrt{\frac{(l+m+1)(l+m+2)}{(2l+3)(2l+1)}},\quad D_1^m=\sqrt{\frac{(l-m)(l+m-1)}{(2l+1)(2l-1)}},$$

$$\mathcal{E}_1^m=\sqrt{\frac{(l-m+1)(l-m+2)}{(2l+3)(2l+1)}},\quad F_1^m=\sqrt{\frac{(l+m)(l+m-1)}{(2l+1)(2l-1)}}.$$

Using our expansion, the material energy equation, Eq. (2), becomes

$$C_v(T)\frac{\partial T}{\partial t} = -\sigma\left(acT^4 - 2\sqrt{\pi}I_0^0\right). \tag{8}$$

Eqs. (3) and (4) are an infinite system of equations and we must truncate them for numerical computation; we set $I_l^m = 0$ for $l \geqslant n$. We can write the P_n radiative transfer system in a more compact form by defining a vector of the moments of the intensity, $\vec{I}$, and writing the coupling constants as a matrix

$$\frac{1}{c}\frac{\partial \vec{I}}{\partial t} + \left(\mathbf{A}_x\frac{\partial}{\partial x} + \mathbf{A}_z\frac{\partial}{\partial z}\right)\vec{I} + \sigma\vec{I} = \sigma\frac{acT^4}{2\sqrt{\pi}}\delta_{l0}\delta_{m0} + \frac{Q}{2\sqrt{\pi}}\delta_{l0}\delta_{m0}, \tag{9}$$

$$C_v(T)\frac{\partial T}{\partial t} = -\sigma\left(acT^4 - 2\sqrt{\pi}I_0^0\right), \tag{10}$$

where we have used the Kronecker-delta notation $\delta_{l0}\delta_{m0}$ to denote terms that appear in the $l = m = 0$ equation.

3. Free-streaming limit and negative solutions

The P_n equations are rotationally invariant, linear, and hyperbolic. These properties of the P_n approximation lead to negative solutions in the free-streaming limit. Below we prove a theorem that demonstrates this point. We note that the theorem deals with the free-streaming limit, and therefore, it applies to any type of neutral particle transport.

Theorem. *Suppose that the discretized transport equation in the source-free, streaming limit is linear and of the form*

$$\frac{\partial \vec{I}}{\partial t} + A_x\frac{\partial \vec{I}}{\partial x} + A_y\frac{\partial \vec{I}}{\partial y} + A_z\frac{\partial \vec{I}}{\partial z} = 0,$$

where $\vec{I}$ is a vector of dependent variables that represent the angular information (e.g. intensity moments in the spherical harmonics expansion). Suppose further that this equation is linear, rotationally invariant, and hyperbolic. Then there exist positive, isotropic initial data in 2D and 3D for which the radiation energy density at subsequent times becomes negative.

Proof. Let $N+1$ be the number of elements of the vector $\vec{I}$. For the sake of this proof we label the elements of vector $\vec{I}$ as I_i, $i = 0, 1, 2, \ldots, N$. Without loss of generality, we can assume that the radiation energy density is proportional to one element of the vector $\vec{I}$, and in particular $E = kI_0$.

Consider an infinite system with the initial condition $I_0(x, y, z, t = 0) = \delta(x)\delta(y)\delta(z)$ and all other angular variables initially zero, $I_i(x, y, z, 0) = 0$, $i \geqslant 1$. Because of rotational invariance $I_0(x, y, z, t)$ generated by this initial data must be of the form $I_0(r, t)$ where $r = \sqrt{x^2 + y^2 + z^2}$ (note that this simple r dependance does not hold for the higher angular moments). Denote the radiation energy density solution for this problem $E_{\mathrm{pt}}(r, t) = kI_0(r, t)$.

With this solution we can use linear superposition to construct the radiation energy density part of the solution to any problem with initial data for the form $I_0(x, y, z, 0) = G(x, y, z)$ and $I_i(x, y, z, 0) = 0$, using

$$E(x, y, z, t) = \int G(x', y', z')E_{\mathrm{pt}}\left(\sqrt{(x - x')^2 + (y - y')^2 + (z - z')^2}, t\right)\mathrm{d}x'\,\mathrm{d}y'\,\mathrm{d}z'. \tag{11}$$

For the initial data $G(x, y, z) = \delta(z)$ we have

$$E(x, y, z, t) = E(z, t) = \int_{-\infty}^{\infty}\int_{-\infty}^{\infty} E_{\mathrm{pt}}\left(\sqrt{(x - x')^2 + (y - y')^2 + z^2}, t\right)\mathrm{d}x'\,\mathrm{d}y' \tag{12}$$

$$= 2\pi\int_0^{\infty} E_{\mathrm{pt}}\left(\sqrt{\Delta r^2 + z^2}, t\right)r\,\mathrm{d}r \tag{13}$$

$$= 2\pi\int_z^{\infty} E_{\mathrm{pt}}(\rho, t)\rho\,\mathrm{d}\rho. \tag{14}$$

Differentiating this we have that

$$E_{\mathrm{pt}}(z,t) = -\frac{1}{2\pi z}\frac{\mathrm{d}E(z,t)}{\mathrm{d}z}\bigg|_{z=\Delta r} \tag{15}$$

and we can therefore compute $E_{\mathrm{pt}}(r,t)$ from the slab geometry problem with initial data $E_0(z,0) = \delta(z)$.

Because the discrete equations are hyperbolic, by definition A_z has distinct real eigenvalues and a complete linearly independent set of eigenvectors. Let Q be the matrix that diagonalizes A_z, so that $\Lambda = QA_ZQ^{-1}$ is a diagonal matrix with real diagonal matrix elements λ_i. Consider then the slab geometry problem

$$\frac{\partial \vec{I}}{\partial t} + A_z\frac{\partial \vec{I}}{\partial z} = 0 \tag{16}$$

with initial data

$$\begin{pmatrix} I_0(z,0) \\ I_1(z,0) \\ \vdots \\ I_N(z,0) \end{pmatrix} = \begin{pmatrix} \delta(z) \\ 0 \\ \vdots \\ 0 \end{pmatrix}. \tag{17}$$

Applying Q we have that

$$\frac{\partial Q\vec{I}}{\partial t} + QA_zQ^{-1}\frac{\partial Q\vec{I}}{\partial z} = 0 \tag{18}$$

and the ith component equation is

$$\frac{\partial Q\vec{I}_i}{\partial t} + \lambda_i\frac{\partial \cdot Q\vec{I}_i}{\partial z} = 0, \tag{19}$$

where $Q\vec{I}_i$ denotes the ith component of $Q\vec{I}$. This shows that each characteristic variable satisfies a linear advection equation with characteristic speed λ_i. The solution of these advection equations is

$$Q\vec{I}_i(z,t) = f_i(z-\lambda_i t), \tag{20}$$

where $f_i(z) = Q\vec{I}_i(z,0)$ is initial data. Because

$$\begin{pmatrix} f_0(z) \\ f_1(z) \\ \vdots \\ f_N(z) \end{pmatrix} = Q\begin{pmatrix} \delta(z) \\ 0 \\ \vdots \\ 0 \end{pmatrix}, \tag{21}$$

we have that $f_i(z) = Q_{i,0}\delta(z)$ and all the f_i's are delta distributions.

Transforming back to $I(z,t)$ we have the solution of the one-dimensional pulsed source problem as $\vec{I} = Q^{-1}Q\vec{I}$ and so

$$I_i(z,t) = \sum_{j=0}^{N}[Q^{-1}]_{i,j}f_j(z-\lambda_j t) = \sum_{j=0}^{N}[Q^{-1}]_{i,j}Q_{j,0}\delta(z-\lambda_j t). \tag{22}$$

Therefore, the radiation energy density in Eq. (15) is of the form

$$E(z,t) = kI_0(z,t) = \sum_{j=0}^{N} a_j\delta(z-\lambda_j t). \tag{23}$$

where $a_j = k[Q^{-1}]_{0,j}Q_{j,0}$.

Because the discrete model is hyperbolic, the radiation energy density for this delta function initial condition is simply a set of N delta functions traveling away from the origin at distinct speeds λ_i.

Differentiating this we have that

$$E_{\mathrm{pt}}(r,t) = -\frac{1}{2\pi z}\frac{\mathrm{d}E(z,t)}{\mathrm{d}z}\bigg|_{z=\Delta r} = -\frac{1}{2\pi z}\sum_{j=0}^{N} a_j \delta'(z-\lambda_j t). \tag{24}$$

The distribution $\delta'(z)$ is not a positive distribution (for a positive function f the integral $\int \delta'(z)f(z)\,\mathrm{d}r = -f'(0)$ need not be positive); it is this that will lead to negative solutions. With the intensity due to a point initial condition in hand we can write the general solution for any initial condition as

$$E(x,y,z,t) = -\sum_{j=0}^{N}\frac{a_j}{2\pi}\int G(x',y',z')\frac{\delta'\left(\sqrt{(x-x')^2+(y-y')^2+(z-z')^2}-\lambda_j t\right)}{\sqrt{(x-x')^2+(y-y')^2+(z-z')^2}}\,\mathrm{d}x'\,\mathrm{d}y'\,\mathrm{d}z' \tag{25}$$

Setting the origin of a spherical coordinate system $(\rho,\widehat{\Omega})$ at $(x,y,z)=\mathbf{r}$ we have $(x',y',z')=\mathbf{r}'=\mathbf{r}+\rho\widehat{\Omega}$ and we can write this integral as

$$E(\mathbf{r},t) = -\sum_{j=0}^{N}\frac{a_j}{2\pi}\int G(\mathbf{r}+\rho\widehat{\Omega})\frac{\delta'(\rho-\lambda_j t)}{\rho}\,\rho^2\,\mathrm{d}\rho\,\mathrm{d}\widehat{\Omega} \tag{26}$$

$$= -\sum_{j=0}^{N}\frac{a_j}{2\pi}\int G(\mathbf{r}+\rho\widehat{\Omega})\delta'(\rho-\lambda_j t)\rho\,\mathrm{d}\rho\,\mathrm{d}\widehat{\Omega} \tag{27}$$

$$= \sum_{j=0}^{N}\frac{a_j}{2\pi}\int_{4\pi}\frac{d}{d\rho}(\rho G(\mathbf{r}+\rho\widehat{\Omega}))_{\rho=\lambda_j t}\,\mathrm{d}\widehat{\Omega}. \tag{28}$$

Evaluating this solution at $\mathbf{r}=0$ we have

$$E(0,t) = \sum_{j=0}^{N}\frac{a_j}{2\pi}\int_{4\pi}[\lambda_j t\,\widehat{\Omega}\cdot\nabla G(\lambda_j t\widehat{\Omega}) + G(\lambda_j t\widehat{\Omega})]\mathrm{d}\widehat{\Omega}. \tag{29}$$

This expression says that the solution at some point (the origin in this case), is given by a sum over the various waves speeds λ_j, with each wave speed contributing an amount that depends on the integral over a sphere of radius $\lambda_j t$. Note here that the integrand on the spherical surface of radius $\lambda_j t$ depends on both the initial data on that surface and also on the gradient of the initial data on that surface. The former contribution will always be positive, but the latter contribution can be positive or negative. Because these two contributions can be of arbitrary sign and magnitude, the net contribution to E can be negative, zero, or positive. Based on this, we can easily construct initial data that will produce a negative scalar intensity at the origin.

Consider a rotationally invariant initial condition where G depends only on the magnitude of its argument; the gradient of G is then radial with magnitude that will be denoted G', and $\widehat{\Omega}$ is also radial, so $\widehat{\Omega}\cdot\nabla G = G'$. Then

$$E(0,t) = \sum_{j=0}^{N}\frac{a_j}{2\pi}\int_{4\pi}[\lambda_j t G'(\lambda_j t) + G(\lambda_j t)]\,\mathrm{d}\widehat{\Omega} \tag{30}$$

$$= \sum_{j=0}^{N} 2a_j[\lambda_j t G'(\lambda_j t) + G(\lambda_j t)]. \tag{31}$$

In this case the intensity at the origin at any fixed time depends simply on the value and the derivative of the initial data at a finite set of distances from the origin.

Select now spherically symmetric initial data representing a thin ring of initial particles near radius 1, specifically

$$G(r) = \begin{cases} 1-\frac{(r-1)^2}{\epsilon^2}, & |r-1|\leqslant\epsilon, \\ 0, & \text{otherwise.}\end{cases} \tag{32}$$

Now pick any one positive wave speed λ_k, and consider times near $t_k = 1/\lambda_k$, specifically $t = t_k + \delta$ where $\delta = \pm\epsilon/2$. For ϵ sufficiently small only the wave speed λ_k will contribute, because $G(\lambda_j t) = G(\lambda_j/\lambda_k + \lambda_j\delta) = 0$ for all other wavespeeds with $j \neq k$. Thus

$$E(0, t_k + \delta) = 2a_k[G'(1 + \delta\lambda_k) + G(1 + \delta\lambda_k)], \tag{33}$$

$$= 2a_k[-2\delta\lambda_k/\epsilon^2 + (1 - (\delta\lambda_k)^2/\epsilon^2)], \tag{34}$$

$$= 2a_k[1 \mp \lambda_k/\epsilon - \lambda_k^2/4]. \tag{35}$$

For ϵ sufficiently small we can make this either positive or negative, by selecting one of the signs for $\delta = \pm\epsilon/2$. Thus, no matter the sign of a_k, we can construct an initial condition that will cause the scalar flux to become negative in 3D.

To show that the 2D solution can become negative, we will integrate a point source over an infinite line located at $x = y = 0$. Using Eq. (24), we get the 2D solution as

$$E(x, y, t) = -\sum_{j=0}^{N} \frac{a_j}{\pi} \int_0^\infty \frac{\delta'(\sqrt{x^2 + y^2 + z^2} - \lambda_j t)}{\sqrt{x^2 + y^2 + z^2}}\, \mathrm{d}z. \tag{36}$$

To compute this solution we change variables to $r = \sqrt{x^2 + y^2 + z^2}$, leading to

$$E(x, y, t) = -\sum_{j=0}^{N} \frac{a_j}{\pi} \int_{\sqrt{x^2+y^2}}^\infty \frac{\delta'(r - \lambda_j t)}{3\sqrt{r^2 - x^2 - y^2}}\, \mathrm{d}r. \tag{37}$$

Noting that

$$\delta'(r - \lambda_j t) = -\frac{\partial}{\partial t}\frac{1}{\lambda_j}\delta(r - \lambda_j t), \tag{38}$$

the 2D solution becomes

$$E(x, y, t) = \sum_{j=0}^{N} \frac{a_j}{\lambda_j \pi} \frac{\partial}{\partial t} \int_{\sqrt{x^2+y^2}}^\infty \frac{\delta(r - \lambda_j t)}{3\sqrt{r^2 - x^2 - y^2}}\, \mathrm{d}r = \sum_{j=0}^{N} \frac{a_j}{\lambda_j \pi} \frac{\partial}{\partial t} \left(\frac{H(\lambda_j t - \sqrt{x^2 + y^2})}{3\sqrt{\lambda_j^2 t^2 - x^2 - y^2}} \right)$$

$$= \sum_{j=0}^{N} \frac{a_j}{3\pi\lambda_j} \left(\frac{\delta\left(\sqrt{x^2 + y^2} - \lambda_j t\right)}{\sqrt{\lambda_j^2 t^2 - x^2 - y^2}} - \frac{t\lambda_j^2 H(\lambda_j t - \sqrt{x^2 + y^2})}{(\lambda_j^2 t^2 - x^2 - y^2)^{3/2}} \right), \tag{39}$$

where $H(x)$ is the Heaviside step function. This solution is negative for either sign of a_j, hence the scalar flux can become negative in 2D. □

The main consequence of this theorem is that for any order P_n expansion, there exists a problem where that approximation will give a negative radiation energy density. The theorem does not state how severe the magnitude of the negative part of the solution will be, nor does it say anything about the behavior or existence of negative energy density in problems with a background material. Also, the theorem does not state what order of expansion we need to have a positive solution for a given problem of interest. These cases we will explore with numerical results in the following sections.

The theorem does say what must be done to "fix" the P_n method. There are four ingredients the theorem relied on. The plane-to-point transform was valid because the P_n equations are rotationally invariant and linear. The delta functions which led to negative solutions are a consequence of the hyperbolic structure of the P_n equations and our ability to isolate the contribution of each wave speed was a consequence of having a finite number of degrees of freedom in the angular variables. This means that if we want to guarantee that the solution given by a P_n method will be positive, we must give up one of these four properties: linearity, rotational invariance, hyperbolicity, or finite angular resolution. Obviously, we cannot give up finite dimensionality if we want to do computer simulations; so there are really only three possibilities. This is unfortunate because the transport equation is linear, rotationally invariant and hyperbolic.

Other methods satisfy this give-and-take in different ways. Diffusion methods give up hyperbolicity by allowing information to travel infinitely fast. This eliminates the delta functions and gives diffusion positivity. Discrete ordinates methods with Gaussian quadrature give the same delta function solutions in slab geometry as P_n methods. However, the discrete ordinates equations are not rotationally invariant so the transform in Eq. (24) does not apply.[3] This lack of rotational invariance leads to the ray effects seen in discrete ordinates solutions [9]. This makes the choice of dropping the rotational invariance of the P_n approach undesirable.

It would be possible to drop linearity through a nonlinear closure. The standard P_n equations are closed by assuming $I^m_{n+1} = 0$. A nonlinear closure would attempt to construct this moment using the other moments that are known. One potentially promising closure is the Minerbo maximum entropy closure which determines the unknown moment using physical arguments regarding the equilibriation of the intensity in angle [5,10]. It should be noted that linear closures derived based on some assumed form for the intensity [11] will not resolve the problem unless they give up hyperbolicity.

Another possible remedy could be to make a diffusion-like approximation in the highest moments in the P_n equations. This would lose the hyperbolic character in the P_n equations, yet how this would actually effect the physics is unknown. It is possible that this approach would only seriously affect the higher moments in the P_n equations without harming the lower moments (which are the most important moments).

4. The finite-volume discretization of the P_n equations for radiative transfer

We will now present a numerical method that we will use to explore how the P_n equations behave on problems outside the scope of the theorem. To begin our spatial discretization, we average Eqs. (9) over a rectangular spatial cell of size $(\Delta x, \Delta z)$ to get

$$\frac{1}{c}\frac{\partial \vec{I}_{i,j}}{\partial t} + \frac{1}{\Delta x}\mathbf{A}_x\left(\vec{I}_{i+1/2,j} - \vec{I}_{i-1/2,j}\right) + \frac{1}{\Delta z}\mathbf{A}_z\left(\vec{I}_{i,j+1/2} - \vec{I}_{i,j-1/2}\right) + \sigma\vec{I}_{i,j} = \sigma\frac{acT^4_{i,j}}{2\sqrt{\pi}}\delta_{l0}\delta_{m0} + \frac{Q_{i,j}}{2\sqrt{\pi}}\delta_{l0}\delta_{m0}, \tag{40}$$

$$C_v(T_{i,j})\frac{\partial T_{i,j}}{\partial t} = -\sigma\left(acT^4_{i,j} - 2\sqrt{\pi}I^0_{0,i,j}\right). \tag{41}$$

The subscripts (i, j) denote the average value in cell i, j where $((i + 1/2)\Delta x, (j + 1/2)\Delta z)$ is the center of cell (i, j). We make the approximation that the temperature is constant within each cell with the cell-average given by

$$T_{i,j} = \frac{1}{\Delta V}\int_{\Delta v} \mathrm{d}V T. \tag{42}$$

We use Eq. (42) to approximate the blackbody source:

$$T^4_{i,j} = \left(\frac{1}{\Delta V}\int_{\Delta V}\mathrm{d}V T\right)^4 \tag{43}$$

$$= \frac{1}{\Delta V}\int_{\Delta V}\mathrm{d}V T^4 + \mathrm{O}(\Delta V^2). \tag{44}$$

Hence, approximating the temperature as constant in a cell contributes a second-order error. Such an approach has been used before in radiation diffusion methods [12]. In our method we solve for (and store) $T_{i,j}$ and use it to compute $T^4_{i,j}$.

Eq. (40) needs a relation to determine the value at a cell boundary (the half-integer subscripts) in terms to cell-average quantities. We do this by solving a Riemann problem at each interface to get [6]

$$\mathbf{A}_x\vec{I}_{i+1/2,j} = \frac{1}{2}\mathbf{A}_x(\vec{I}^x_{i+1,j} + \vec{I}^x_{i,j}) - \frac{1}{2}|\mathbf{A}_x|(\vec{I}^x_{i+1,j} - \vec{I}^x_{i,j}), \tag{45}$$

$$\mathbf{A}_z\vec{I}_{i,j+1/2} = \frac{1}{2}\mathbf{A}_z(\vec{I}^z_{i,j+1} + \vec{I}^z_{i,j}) - \frac{1}{2}|\mathbf{A}_z|(\vec{I}^z_{i,j+1} - \vec{I}^z_{i,j}), \tag{46}$$

[3] Discrete ordinates solutions can sometimes have negative values for the radiation energy density, but this is a numerical effect caused by some spatial discretizations [2], whereas the P_n equations have these negatives in the spatially continuous limit.

where

$$|\mathbf{A}| = \sum_k \vec{r}_k |\lambda_k| \vec{l}_k, \tag{47}$$

with $\vec{r}_k$ and $\vec{l}_k$ being the kth right and left eigenvectors of $\mathbf{A}$ with corresponding eigenvalue λ_k. In Eqs. (45) and (46) we have included a slope reconstruction term for the moments of the intensity

$$\vec{I}^x_{i,j} = \vec{I}_{i,j} + \frac{\Delta x}{2} m^x_{i,j}, \tag{48}$$

$$\vec{I}^z_{i,j} = \vec{I}_{i,j} + \frac{\Delta z}{2} m^z_{i,j}. \tag{49}$$

Here $m_{i,j}$ is a slope in the x or z direction computed by using the values in the neighboring cells and a minmod limiter [13]. In the x direction for constant Δx this slope is calculated for each moment using the formula

$$m^{m,x}_{l,i,j} = \begin{cases} \min(|m_+|, |m_-|), & m_+ m_- > 0, \\ 0, & \text{otherwise}, \end{cases} \tag{50}$$

where

$$m_+ = \frac{1}{\Delta x}(I^m_{l,i+1,j} - I^m_{l,i,j}), \quad m_- = \frac{1}{\Delta x}(I^m_{l,i,j} - I^m_{l,i-1,j}). \tag{51}$$

The slope is computed in a similar fashion in the z direction. The formula for the cell edge values given in Eqs. (45) and (46) is a combination of the average between the cells on either side of the interface (the näive way of computing this value) minus some dissipation. The dissipation is of the form that it causes positive characteristics to move information in the positive direction (e.g. from $\vec{I}_{i,j} \to \vec{I}_{i+1/2,j}$) and negative characterisitics to flow in the negative direction (e.g. from $\vec{I}_{i+1,j} \to \vec{I}_{i+1/2,j}$). In this sense the discretization is upwinded: it respects the underlying physics.

We note that the slope in each cell is constructed in a nonlinear fashion. This is necessary to avoid artificial oscillations in the solution. The minmod limiter could be replaced by a smoother limiting function (such as Van Leer's harmonic mean limiter [14] as done by Brunner and Holloway [5,4]). However, it was shown by McClarren [6] that using the minmod limiter is numerically advantageous for use in an implicit time-integration scheme because it is linear after the choice of stencil is made, and the choice of stencil can be predicted beforehand by solving a simpler system.

The spatial discretization outlined above does not limit to a valid diffusion discretization when a mean-free path is not resolved. As the spatial cells get optically thick the numerical dissipation has a constant magnitude. In the limit of optically thick cells the leading-order "diffusion" equation in the limit of optically thick cells is a discrete approximation to $\nabla^2 I^0_0 = 0$. This result was shown by the authors for linear transport in Ref. [15] and has been discussed by other researchers [16]. Hence, in using this discretization we must have the cell size resolve a mean-free path. For the purposes of exploring when the P_n equations give negative energy densities we will be interested in studying optically thin systems, therefore, the performance of the method in the diffusion limit is a separate issue. Nevertheless, we stress that for a purposes of a production radiative transfer code robustness in the diffusion limit is vital.

The final piece of our discretization is time integration. We will use the backward Euler method for this. With this method our fully discretized equations become

$$\begin{aligned} &\frac{1}{c}\frac{\vec{I}^{n+1}_{i,j} - \vec{I}^n_{i,j}}{\Delta t} + \frac{1}{\Delta x}\mathbf{A}_x(\vec{I}^{n+1}_{i+1/2,j} - \vec{I}^{n+1}_{i-1/2,j}) + \frac{1}{\Delta z}\mathbf{A}_z(\vec{I}^{n+1}_{i,j+1/2} - \vec{I}^{n+1}_{i,j-1/2}) + \sigma\vec{I}^{n+1}_{i,j} \\ &\quad = \sigma\frac{ac(T^{n+1}_{i,j})^4}{2\sqrt{\pi}}\delta_{l0}\delta_{m0} + \frac{Q^{n+1}_{i,j}}{2\sqrt{\pi}}\delta_{l0}\delta_{m0}, \end{aligned} \tag{52}$$

$$\frac{C_v(T^{n+1}_{i,j})T^{n+1}_{i,j} - C_v(T^n_{i,j})T^n_{i,j}}{\Delta t} = -\sigma\left(ac(T^{n+1}_{i,j})^4 - 2\sqrt{\pi}I^{0,n+1}_{0,i,j}\right). \tag{53}$$

Note these equations are nonlinear because of the slope reconstruction and the material energy terms.

5. Boundary conditions

The simplest way to specify a boundary condition for our discretization is using ghost cells. In this implementation of a boundary condition, cells are placed outside the physical system in which we specify the value of the moments of the intensity. Then our upwind discretization will automatically move only the appropriate incoming information into the problem. Brunner and Holloway showed that the Mark boundary condition is trivial to implement using ghost cells [5].

We will now show how this ghost cell framework can be used to specify a reflecting boundary. To begin we will show what a reflecting boundary means in P_n. This type of boundary condition causes the system boundary to reflect particles impinging on the boundary interface. The particles hitting the boundary are to be reflected with the same angle relative to the outward normal to the interface. The relation between θ_i and θ_r, taking into account direction, is $\theta_r = \pi - \theta_i$. For an incident particle with direction $\widehat{\Omega_i}$, the angle between the outward normal and Ω_i is given by $\widehat{\Omega_i} \cdot \hat{n} = \cos\theta_r$ and the reflected angle is then given by $\widehat{\Omega_r} \cdot \hat{n} = \cos(\pi - \theta_i) = -\cos\theta_i$. Therefore the intensity at the boundary is symmetric in the cosine of the polar angle with respect to $\hat{n}$

$$I(\cos\theta_i) = I(-\cos\theta_i) \quad \text{for } \cos\theta_i > 0. \tag{54}$$

The incident direction of a particle in terms of Cartesian coordinates (x, z) is

$$\widehat{\Omega}_i' = \left(\sqrt{1-\mu^2}\cos\phi, \mu\hat{k}\right). \tag{55}$$

The reflecting boundary condition for general inward normal is a linear combination of the boundary conditions for each of the x and z directions. We will now derive the boundary conditions for each of these directions.

5.1. The Z direction

If the outward normal, $\hat{n}$, equals $\hat{k}$ the boundary condition becomes

$$I(\mu,\phi)_{\mu>0} = I(-\mu,\phi), \tag{56}$$

because $\widehat{\Omega_i} \cdot \hat{n} = \mu$. The intensity at the boundary is an even function of μ. Therefore, the moments of this intensity are given by

$$I^m_{l\text{boundary}} = \int_0^{2\pi} \mathrm{d}\phi \int_{-1}^{1} \mathrm{d}\mu \bar{Y}_1^m I(\mu,\phi) = \begin{cases} I^m_l & l+m \quad \text{even}, \\ 0 & l+m \quad \text{odd}. \end{cases} \tag{57}$$

This is because the associated Legendre functions are odd in μ for $l+m$ odd and they are even if $l+m$ is even.

To impose this boundary condition using ghost cells we will set the boundary flux to be

$$F^m_{l\,\text{Boundary}} = \frac{1}{2}\left(I^m_{l\,\text{interior}} + I^m_{l\,\text{ghost}}\right), \tag{58}$$

with

$$I^m_{l\,\text{ghost}} = \begin{cases} I^m_{l\,\text{interior}} & l+m \quad \text{even}, \\ -I^m_{l\,\text{interior}} & l+m \quad \text{odd}. \end{cases} \tag{59}$$

This type of ghost cell is implemented by modifying the stencil at the boundary to treat each boundary cell as its own ghost cell. Note that Eq. (59) is equivalent to making our scheme a centered-difference (and not upwinded) scheme at the boundary.

5.2. The X direction

For $\hat{n} = \hat{i}$, the incident angle is given by

$$\cos\theta_i = \sqrt{1-\mu^2}\cos\phi. \tag{60}$$

This makes the outgoing (exiting the system) direction $\cos\phi > 0$ or $\phi \in [-\pi/2, \pi/2]$, and the reflected direction $\cos\phi < 0$ or $\phi \in [\pi/2, 3\pi/2]$. The boundary condition is

$$I(\mu,\phi)_{\phi\in[-\pi/2,\pi/2]} = I(\mu,\pi-\phi). \tag{61}$$

This condition requires the value on the boundary to be

$$I^m_{l\,\text{boundary}} = \begin{cases} I^m_l & m \quad \text{even}, \\ 0 & m \quad \text{odd}. \end{cases} \tag{62}$$

Eq. (62) results from the fact that the real part of the spherical harmonics are symmetric under a π radian rotation for m even and are anti-symmetric under that rotation for m odd. These conditions are satisfied using ghost cells by setting the flux at the boundary to

$$F^m_{l\,\text{Boundary}} = \frac{1}{2}\left(I^m_{l\,\text{interior}} + I^m_{l\,\text{ghost}}\right), \tag{63}$$

with

$$I^m_{l\,\text{ghost}} = \begin{cases} I^m_{l\,\text{interior}} & m \quad \text{even}, \\ -I^m_{l\,\text{interior}} & m \quad \text{odd}. \end{cases} \tag{64}$$

6. Implementation

Eqs. (52) and (53) form a system of nonlinear equations. This system could be solved using a Newton–Krylov solver [17]. McClarren, Holloway, et al. showed how a similar system from linear transport could be efficiently solved using a quasi-linear approach [6].

This approach, which we will extend here to the radiative transfer case, centers on the reality that the streaming in the P_n equations is linear; nonlinearities are added only to make the scheme non-oscillatory. The nonlinearities added have discontinuous derivatives, and this type of nonlinearity is difficult for a Newton method to handle. In the case of X-ray transport there are nonlinearities inherent in the physics of the system. However, the streaming of photons is still a linear phenomenon and because of this fact we can use the quasi-linear approach to simplify the nonlinearities added to the radiation streaming.

The quasi-linear approach for Eqs. (52) and (53) is given in Algorithm 1. This algorithm takes advantage of the fact that the minmod limiter is linear once the choice of stencil is determined. In the first step, the system is solved using a slope of zero to calculate the edge values in each cell (a first-order discretization). This gives us information at the forward time step to determine how to reconstruct the slope (i.e. evaluate the cases in Eq. (50)). Once we know how to reconstruct the slope in each cell, the streaming term is linear, and we use this linear streaming term in step three. This approach could not be used with a limiter function that is not linear once the choice of stencil is made. Using this two step approach on the streaming nonlinearity we have eliminated the discontinuous nonlinearity in the streaming discretization.

Algorithm 1. Quasi-linear algorithm for radiative transfer

1. Solve the system

$$\frac{1}{c\Delta t}\vec{I}^*_{i,j} + \frac{1}{\Delta x}\mathbf{A}_x(\vec{I}^*_{i+1/2,j} - \vec{I}^*_{i-1/2,j}) + \frac{1}{\Delta z}\mathbf{A}_z(\vec{I}^*_{i,j+1/2} - \vec{I}^*_{i,j-1/2}) + \sigma^*\vec{I}^*_{i,j} - \frac{1}{2\sqrt{\pi}}\sigma^*(ac(T^*_{i,j})^4)\delta_{l0}$$
$$= \frac{1}{c\Delta t}\vec{I}^n_{i,j} + \frac{1}{2\sqrt{\pi}}Q^*_{i,j}\delta_{l0},$$
$$C_v(T^*_{i,j})\frac{T^*_{i,j}}{\Delta t} + \sigma^*(ac(T^*_{i,j})^4 - 2\sqrt{\pi}I^{0,*}_{0,i,j}) = C_v(T^n_{i,j})\frac{T^n_{i,j}}{\Delta t}$$

with $m^x_{i,j} = m^z_{i,j} = 0$, using Newton–Krylov.

2. Determine the stencil for $m^x_{i,j}$ and $m^z_{i,j}$ using $\vec{I}^*$ to evaluate the cases in Eq. (50).
3. Solve the new system

$$\frac{1}{c\Delta t}\vec{I}^{n+1}_{i,j}+\frac{1}{\Delta x}\mathbf{A}_x(\vec{I}^{n+1}_{i+1/2,j}-\vec{I}^{n+1}_{i-1/2,j})+\frac{1}{\Delta z}\mathbf{A}_z(\vec{I}^{n+1}_{i,j+1/2}-\vec{I}^{n+1}_{i,j-1/2})+\sigma^{n+1}\vec{I}^{*}_{i,j}-\frac{1}{2\sqrt{\pi}}\sigma^{n+1}(ac(T^{n+1}_{i,j})^4)\delta_{l0}$$
$$=\frac{1}{c\Delta t}\vec{I}^{n}_{i,j}+\frac{1}{2\sqrt{\pi}}Q^{n+1}_{i,j}\delta_{l0},$$
$$C_v(T^{n+1}_{i,j})\frac{T^{n+1}_{i,j}}{\Delta t}+\sigma^{n+1}(ac(T^{n+1}_{i,j})^4-2\sqrt{\pi}I^{0,n+1}_{0,i,j})=C_v(T^{n}_{i,j})\frac{T^{n}_{i,j}}{\Delta t}$$

using Newton–Krylov and the stencil for $m^x_{i,j}$ and $m^z_{i,j}$ computed in step 2.

In thermal transport the equations in steps one and three of Algorithm 1 are nonlinear and those steps would be linear only if the material equation and temperature source terms were linearized and the material properties (σ, C_v) were evaluated at the previous time step's temperature. However, the temperature equation is local and only feeds directly into the transport equations for its own cell. For this reason, we treat the material temperature fully nonlinearly and do not lag the material temperatures. To do this we use a Newton–Krylov solver in steps one and three of Algorithm 1. This nonlinear treatment could be modified to use a linearization of the temperature equation. We have not explored linearizing the temperature terms.

McClarren, Holloway, and Brunner used a modified equation analysis [18] to demonstrate that extreme points in the solution move at the same velocity to order Δx^2 in both the high-resolution equations and the first-order discretization [6]. This allows the first step to correctly locate the extreme points so that little error is incurred in this three-step algorithm compared to doing a full nonlinear solve. The streaming operators are the same for linear and thermal transport so their analysis holds for the thermal case.

The first solve uses the previous time-step's result as the initial guess while the final solve takes $\vec{I}^*$ as the guess. While the algorithm involves solving two nonlinear systems, the solution of the second system is made much easier by the use of this initial guess. Our implementation uses the fact that a Newton–Krylov method only needs to perform the action of a matrix times a vector.

The Newton–Krylov method that we use is the NOX package from the Trilinos solver library from Sandia National Laboratories [19]. In NOX we use a matrix-free approximate Jacobian to avoid computing and storing the Jacobian for our system. We precondition the method with an ILU decomposition of the first-order streaming operator.

7. Numerical results

7.1. One-dimensional problems

In one-dimensional problems we do not expect to see negative energy densities, however, we can use such problems to look at how a P_n solution converges to a transport solution and to examine how the numerical method performs.

The first problem we will examine is the Su–Olson finite source problem [20], a problem of thermal transport in normalized units with $C_v \propto T^3$. There is a unit source of radiation for $|z| < 0.5$; the source is turned on at $t = 0$ and left on until $t = 10$. In our results $\sigma = 1$ and $C_v = 4aT^3$. Using this problem we can examine how the P_n equations limit to transport. This is done by comparing different P_n approximations with fine spatial grids and time steps ($\Delta x = 0.015$ and $\Delta t = 0.01$) to the analytic transport solution found by Su and Olson [20]. Figs. 1 and 2 show such comparisons. We see that P_1 does a poor job, yet P_3 performs noticeably better than P_1. In Fig. 2 we can see the effect of the slow P_1 wave speed. P_1 only allows information to propagate at $c/\sqrt{3}$ and on the logarithmic scale we can see that P_1, with only one wave speed, does not propagate information at the correct speed. Some places of the solution have too much energy and others do not have enough. A similar comparison was performed by Olson et al. for P_1 and different flux-limited diffusion, and variable-Eddington factor methods [21]; there is also an analytic solution for the P_1 approximation on this problem [3].

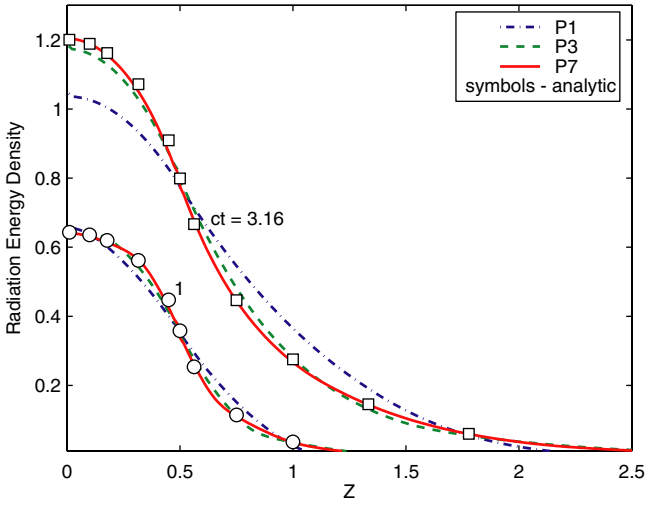

Fig. 1. Comparison of several P_n solutions with $\Delta x = 0.015$ and $\Delta t = 0.01$ to the transport solution for the Su–Olson benchmark.

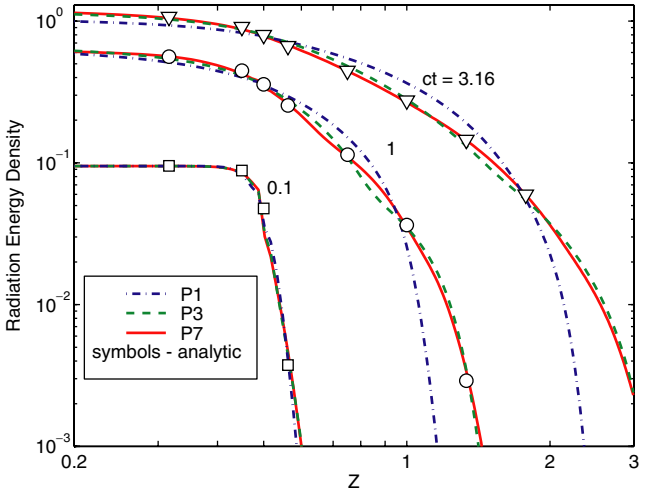

Fig. 2. Comparison of several P_n solutions with $\Delta x = 0.015$ and $\Delta t = 0.01$ to the transport solution for the Su–Olson benchmark on a logarithmic scale.

To quantify the convergence of the P_n solution to transport we examined the L_1 error between the P_n numerical solution and the analytic transport solution at $ct = 1$; this error as function of P_n order is shown in Fig. 3. Between orders 3–9, the P_n solution converges at first order in n to the transport solution.

7.2. Two-dimensional problems

In one-dimensional problems we showed that P_n orders of seven and nine were sufficient to provide a good approximation to the transport solution. Now we will look at some multi-material problems in two dimensions to explore the behavior of the P_n approximation and the consequences of our theorem.

Our first 2D test problem models radiative heating across a vacuum. This problem (see Fig. 4) has a central block of material heated with a source, S, on the right hand side of the material energy equation Eq. (8). The form of S that we use is

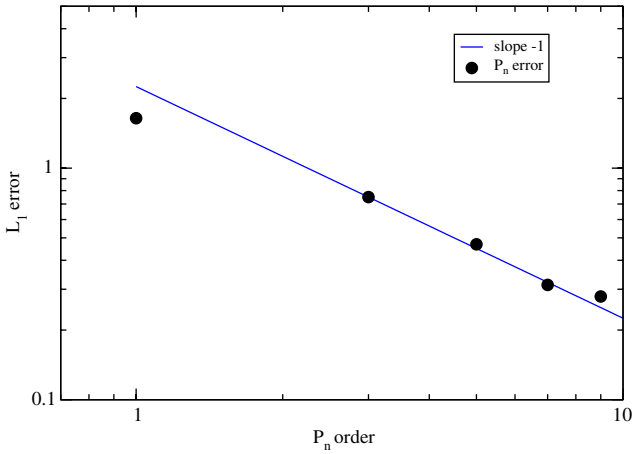

Fig. 3. The L_1 norm of the error between the P_n solution and the transport solution at $ct = 1$.

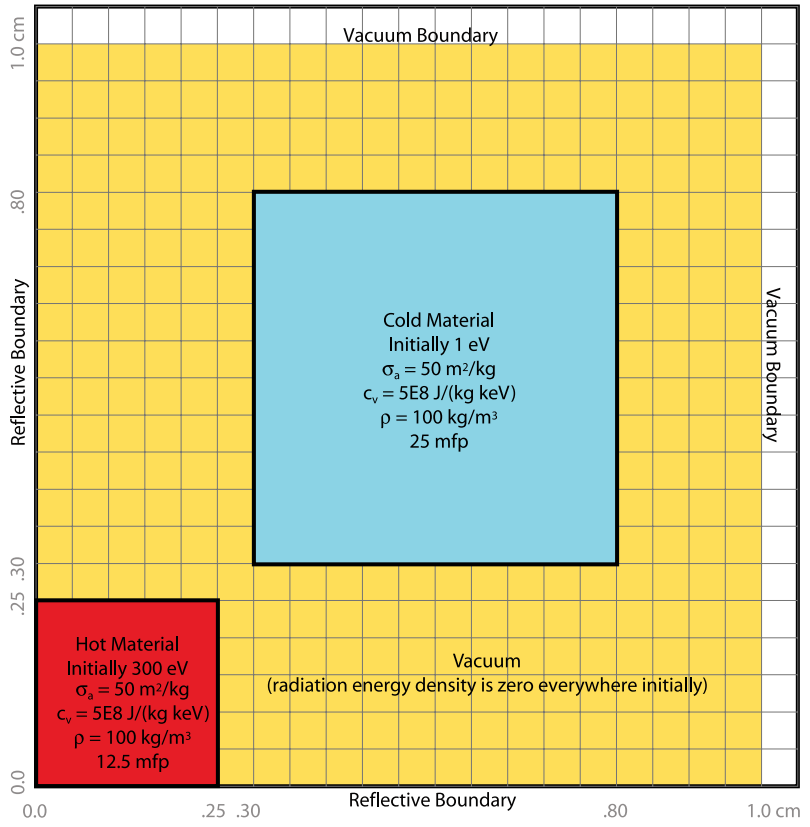

Fig. 4. The problem of a hot block heating cold blocks across a vacuum.

$$S = C_v \dot{T}_s, \tag{65}$$

where $\dot{T}_s$ has units of temperature per second. We do this so we can input the source as a temperature rate. The cold block is not heated and its initial temperature is $T = 1$ eV; at the beginning of the problem there is no radiation field. The blocks are consubstantial with $C_v = 5 \times 10^{10}$ J/m^3/ keV and $\sigma = 5000$ m^{-1}. The reflecting boundaries quadruple the actual size of the problem – there are four of the initially cooler blocks.

This problem is a good indicator of how both the P_n approach and our method will work on realistic problems with materials heating each other across a vacuum. This problem uses a constant heat capacity, making the temperature feedback nonlinear. This particular instance of the problem had the heated block's material source $\dot{T}_s$ given by

$$\dot{T}_s = \begin{cases} \frac{300 \text{ eV}}{(0.5 \text{ ns})^2} t & 0 < t < 0.5 \text{ ns}, \\ \frac{600 \text{ eV}}{0.5 \text{ ns}} - \frac{300 \text{ eV}}{(0.5 \text{ ns})^2} t & 0.5 \text{ ns} < t < 1 \text{ ns}, \\ 0 & \text{otherwise}. \end{cases} \tag{66}$$

$\dot{T}_s$ is defined this way because when the heat source S is integrated over time the total energy put into the problem is

$$C_v \int_0^\infty \mathrm{d}t \dot{T}_s = 1.5 \times 10^{10} \text{ J} \quad \text{for } \Delta t < 0.5 \text{ ns}. \tag{67}$$

In Fig. 5 the energy density from different orders of P_n are shown. For this figure, the radiation temperature was calculated using

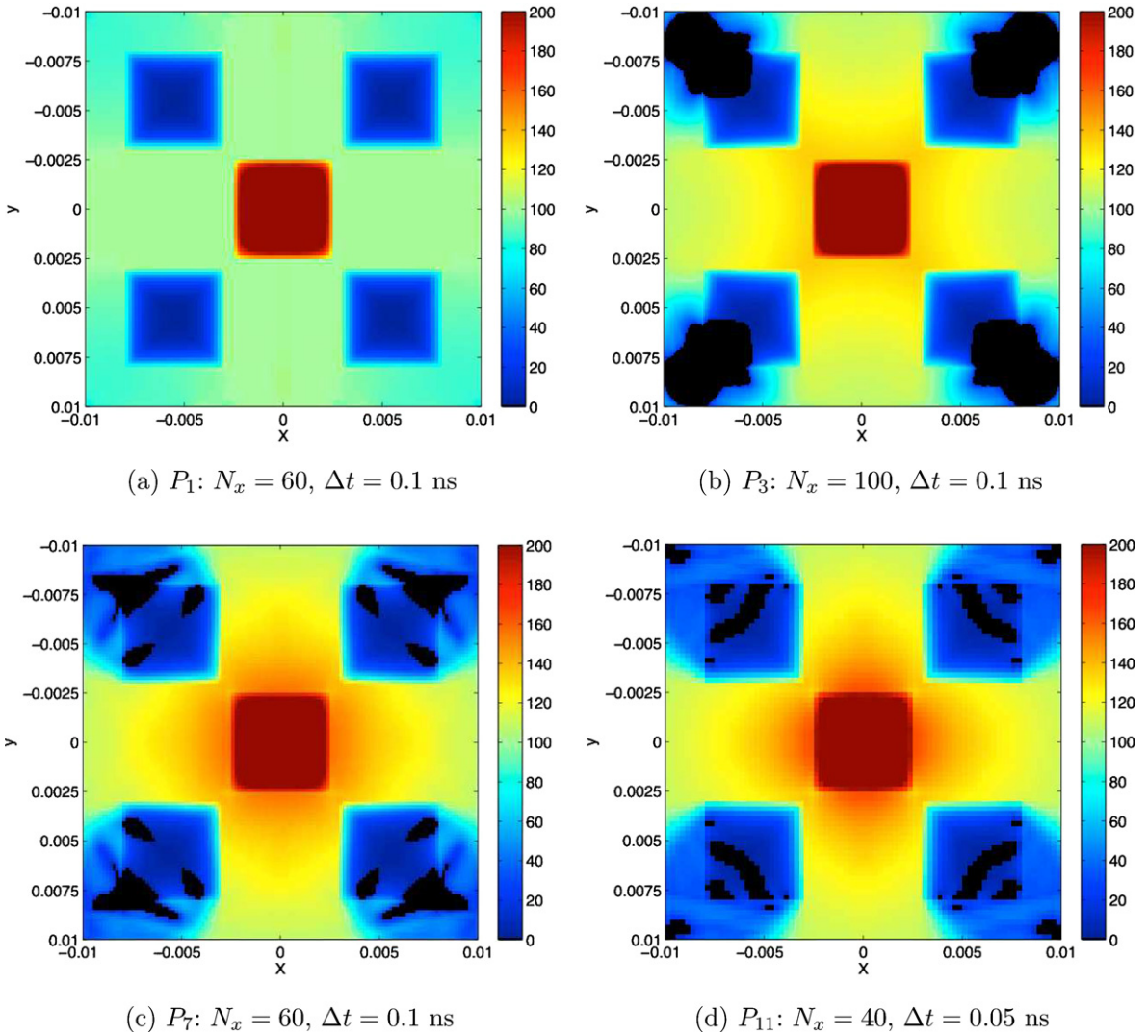

(a) P_1: $N_x = 60$, $\Delta t = 0.1$ ns

(b) P_3: $N_x = 100$, $\Delta t = 0.1$ ns

(c) P_7: $N_x = 60$, $\Delta t = 0.1$ ns

(d) P_{11}: $N_x = 40$, $\Delta t = 0.05$ ns

Fig. 5. Radiation temperature (eV) at 2 ns for the problem of heating across a vacuum using different P_n orders. All problems were run on a Cartesian mesh with $N_x = N_z$. Black colors represent negative radiation temperature.

$$T_r = \mathrm{sign}(E)\sqrt[4]{\frac{|E|}{a}}, \tag{68}$$

because the solutions had negative energy densities. Black in the figure represents negative radiation temperatures. This will give us an estimate of how well a given order can capture the shadow behind the cold blocks. The P_1 solution has no shadow behind the cold block, showing that in P_1 photons non-physically wrap around the cold block. P_3 shows this phenomenon as well but to a lesser extent; a shadow does exist in this solution. Both the P_7 and the P_{11} solutions have a shadow behind the cold block. With the P_7 solution there is some radiation at temperature of 60–89 eV hitting the back of the block. In Fig. 5 all of the solutions with $n > 1$ also have a negative part to the radiation temperature in the shadow region. P_1 has no negatives because it has no shadow. After they appear, the magnitude of these non-physical negatives goes down as n is increased. The P_3 solution has a maximum negative of 63 eV, the P_7 maximum is about 40 eV, and the P_{11} result has a maximum of 31 eV. This trend corresponds to the magnitude of the negative energy density decaying as $O(n^{-1})$, where n is the order of the P_n expansion. The separated positive and negative parts of the P_7 solution are shown in Fig. 6.

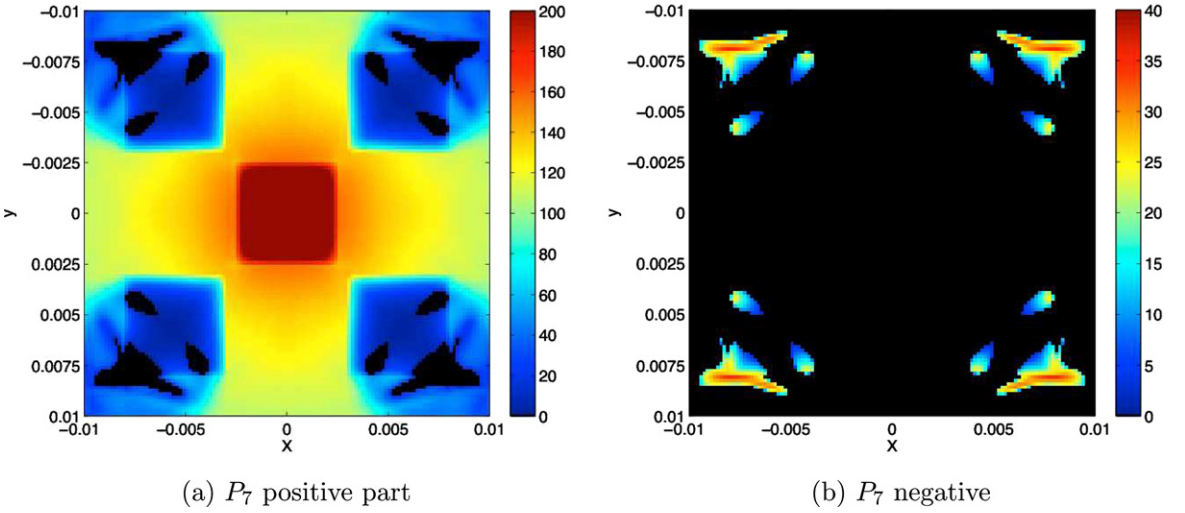

Fig. 6. Comparison of the positive and negative parts of the radiation temperature (eV) for the P_7 solution at 2 ns.

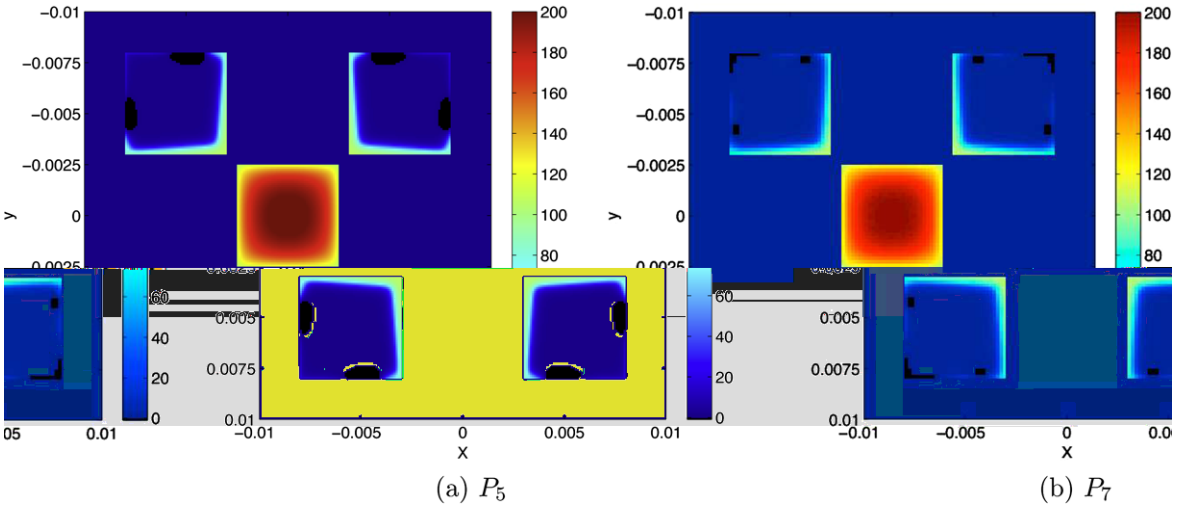

Fig. 7. Material temperatures (eV) at 10ns for P_5 and P_7. The colorscale has any temperature -1 eV or below colored black.

The existence of negative solutions in multi-dimensional problems was predicted by the theorem in Section 3. The real importance of the negative radiation energy density is how it affects the material temperatures. If the radiation did not cause the material temperature to go negative, then the non-physical nature of the negatives would be more of a quirk than a serious drawback. At two nanoseconds the P_1 material temperature remained positive; the maximum negative for was -10.86 eV for P_3, -11.6 eV for P_5, and -0.78 eV for P_7. The P_{11} solution material temperature remained positive. The material temperatures at a later time are shown in Fig. 7. In this figure both P_7 and P_5 have regions of negative material temperature. The P_5 minimum temperature is about -24 eV and the P_7 negative is near -2 eV.

Finally, it should be pointed out that in all of these figures (Figs. 5–7) implicit time stepping was heavily utilized; every solution had the radiation travelling across the entire problem domain multiple times in a time step with CFL numbers ranging from 60 to 150. To justify taking such large time steps we can look at the effect of large time steps on the solution. A study was done on an instance of this problem where the hot block was started at 300 eV rather than ramped up. This is a more difficult problem to simulate because of the large initial difference in radiation and material temperatures. Figs. 8 and 9 show the effect of time-step size on the P_7

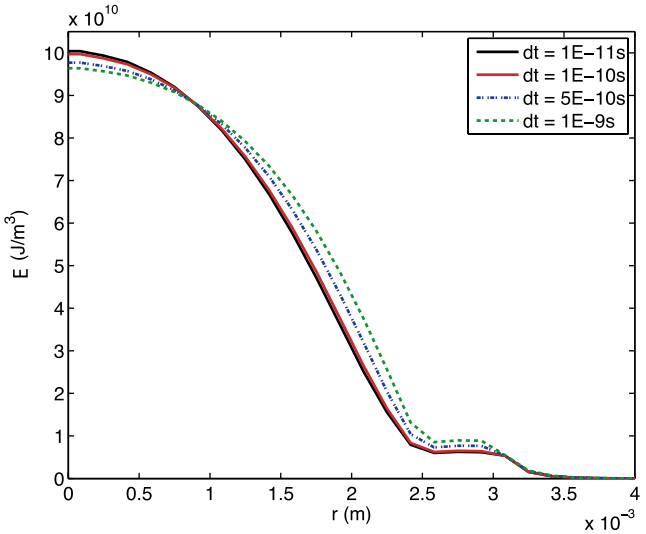

Fig. 8. Effect of time-step size on the P_7 radiation energy density (J/m^3) for the wire problem at 8.5 ns with $\Delta x = 1.6667 \times 10^{-4}$ m.

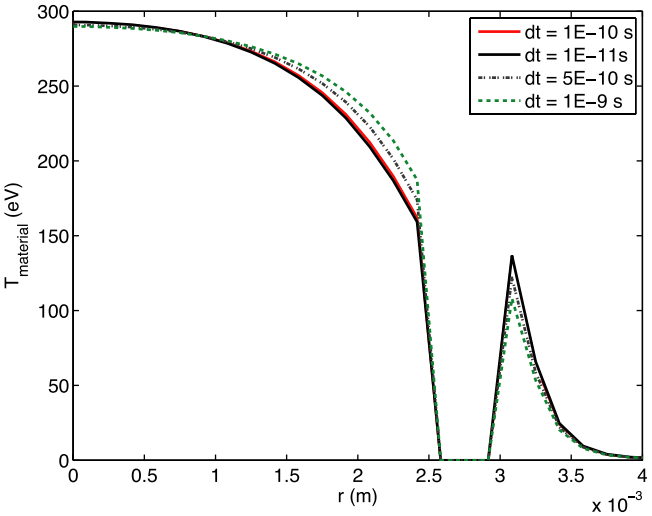

Fig. 9. Effect of time-step size on the P_7 material temperature (eV) at 8.5 ns with $\Delta x = 1.6667 \times 10^{-4}$ m.

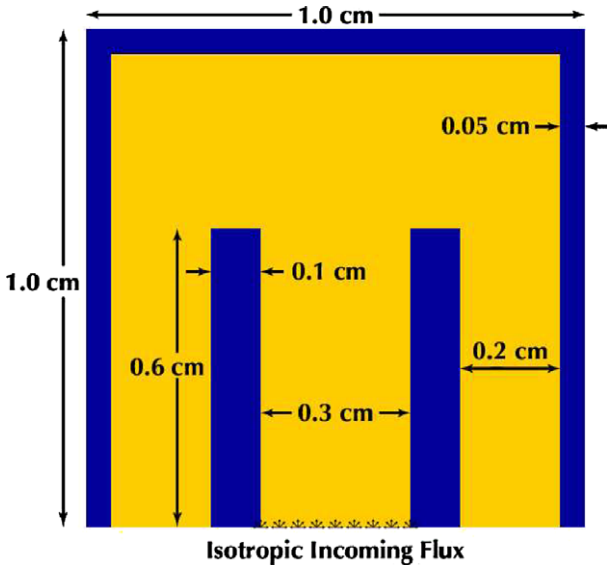

Fig. 10. The "M" problem schematic: the maize colored regions are vacuum and the blue regions are dense material. (For interpretation of the reference in colour in this figure legend, the reader is referred to see the web version of this article.)

solution with $N_x = N_z = 60$. These figures show the lineout along the diagonal from the center of the heated block through the cold block and into the shadow region. In this problem the time scale of the material temperature was as short as about 0.1 ns. These figures show that there is significant time-integration error in both the radiation and material temperature fields when time steps are larger than this material temperature time scale. This is the case for the radiation field even when the time scale of radiation propagation is greater than 100 times shorter than the time step.

Another problem we solved was a modification of the "M" problem [6]. A schematic of this problem is shown in Fig. 10. We modified the original linear problem to give it temperature feedback: the walls of the duct have $C_v = 5 \times 10^{10}$ J/m^3/keV and $\sigma = 5000$ m^{-1}. There is a 300 eV isotropic radiation source entering the middle leg of the duct, and we use the real value of the speed of light. This nonlinear version of the problem produces negative energy densities whereas the purely scattering problem in Ref. [6] did not. Fig. 11 shows the effect of different P_n approximations on the solution at an early time. The P_3 solution has too much energy turning the corner of the duct; the P_7 solution shows less of this effect and displays a cone of radiation near the top of the duct. In the P_3 solution there is a local maximum at the top of the middle leg of the duct. The P_7 solution has "waves" of energy in the outer legs of the duct. At this time, the magnitude of the negatives in the P_3 solution was larger than that in the P_7 solution. However, a greater area of the solution was negative (for both the energy density and material temperature) in the P_7 case.

The solution at a later time, 6 ns, is shown in Fig. 12. Here, we notice that the P_3 creates a "mushroom" of photons near the top of the duct while the P_7 solution maintains a less rounded shape. In terms of material heating, the P_3 solution has significant artificial heating of the outer legs of the duct. The P_7 solution shows much less of this effect. This difference could be important in a problem where the heating of the wall affected some other physical process (e.g. in a radiation-hydrodynamics simulation). Despite having less artificial heating in the outer legs of the duct, the P_7 solution has a larger region of artificial cooling.

Using this problem we can estimate the performance of our implicit method compared with an explicit method. For the P_7 results of this problem, the CFL number is 150. The average number of GMRES iterations in completing a time step is 1000 (approximately 600 in the first linear solve and 400 in the second). If we assume an explicit method runs at a CFL number of 0.9 (just below the CFL limit), then it would take 167 explicit time steps to equal one implicit time step. To make the implicit method more efficient than the explicit method would require an explicit time step to take the same amount of time as six GMRES iterations. We would expect an explicit time step to take as long as several GMRES iterations. This expectation is based

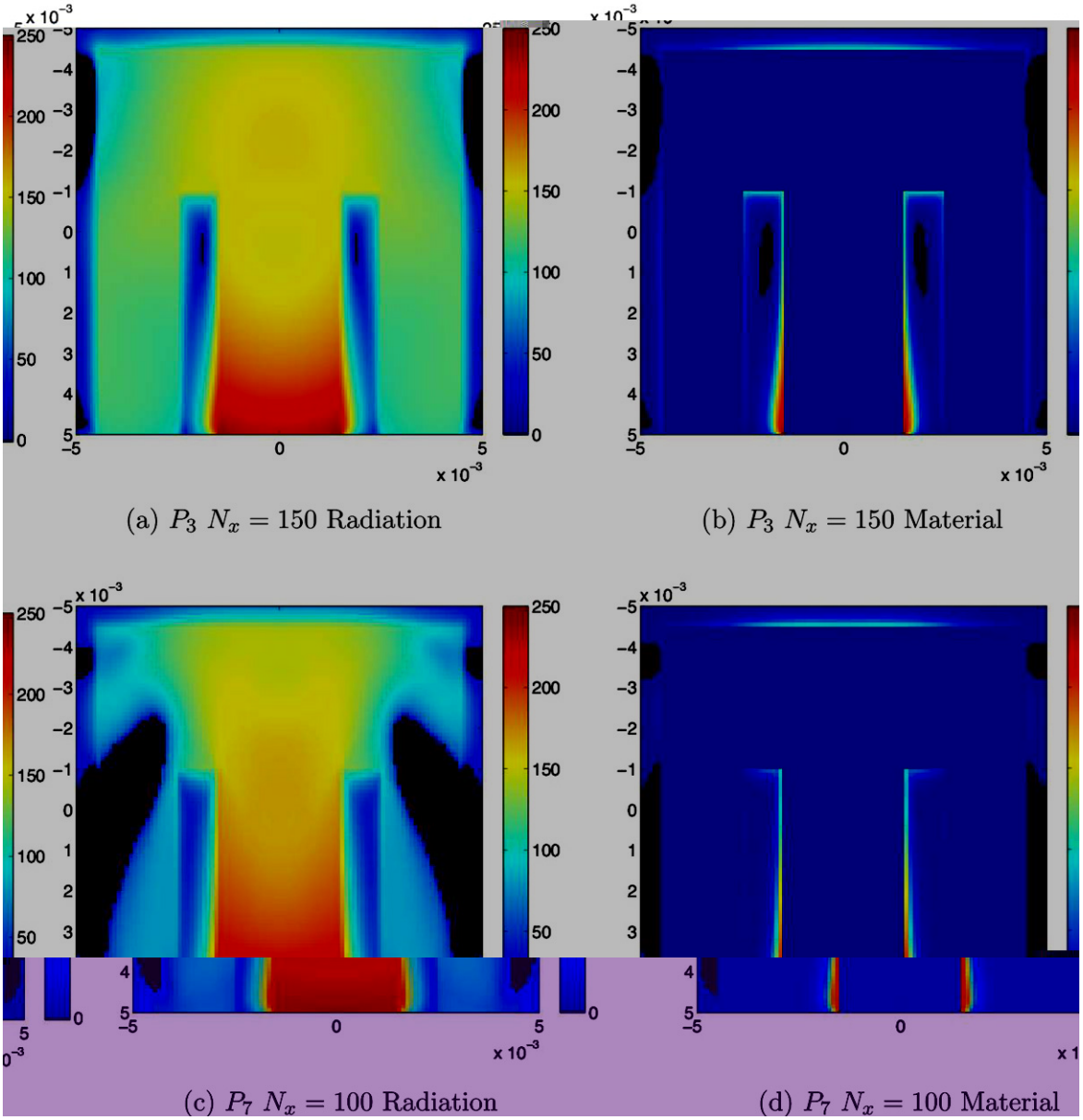

Fig. 11. Radiation and material temperature (eV) at 0.9 ns for the thermal duct problem using different P_n orders. All problems were run on a Cartesian mesh with a time step of $\Delta t = 0.05$ ns.

on the fact that one GMRES iteration requires approximately $O(M)$ operations where M is the number of unknowns in a linear system. An explicit time step would require several iterations on the temperature feedback terms, each roughly equivalent to a GMRES iteration. Also, the process of slope limiting would be about equivalent to a GMRES iteration. Given this back-of-the-envelope calculation the performance of the implicit method is approximately equivalent to the performance of an explicit method. Numerical experiments show that, for CFL numbers in the hundreds, the number of GMRES iterations required by the implicit method is nearly constant as the CFL number changes. This result means that as the spatial grid is refined, the implicit method will perform better than an explicit method.

To date we have not spent a great deal of effort on accelerating the implicit method. The topic of preconditioning the linear systems in the two steps of the quasi-linear method is largely unexplored. If better precon-

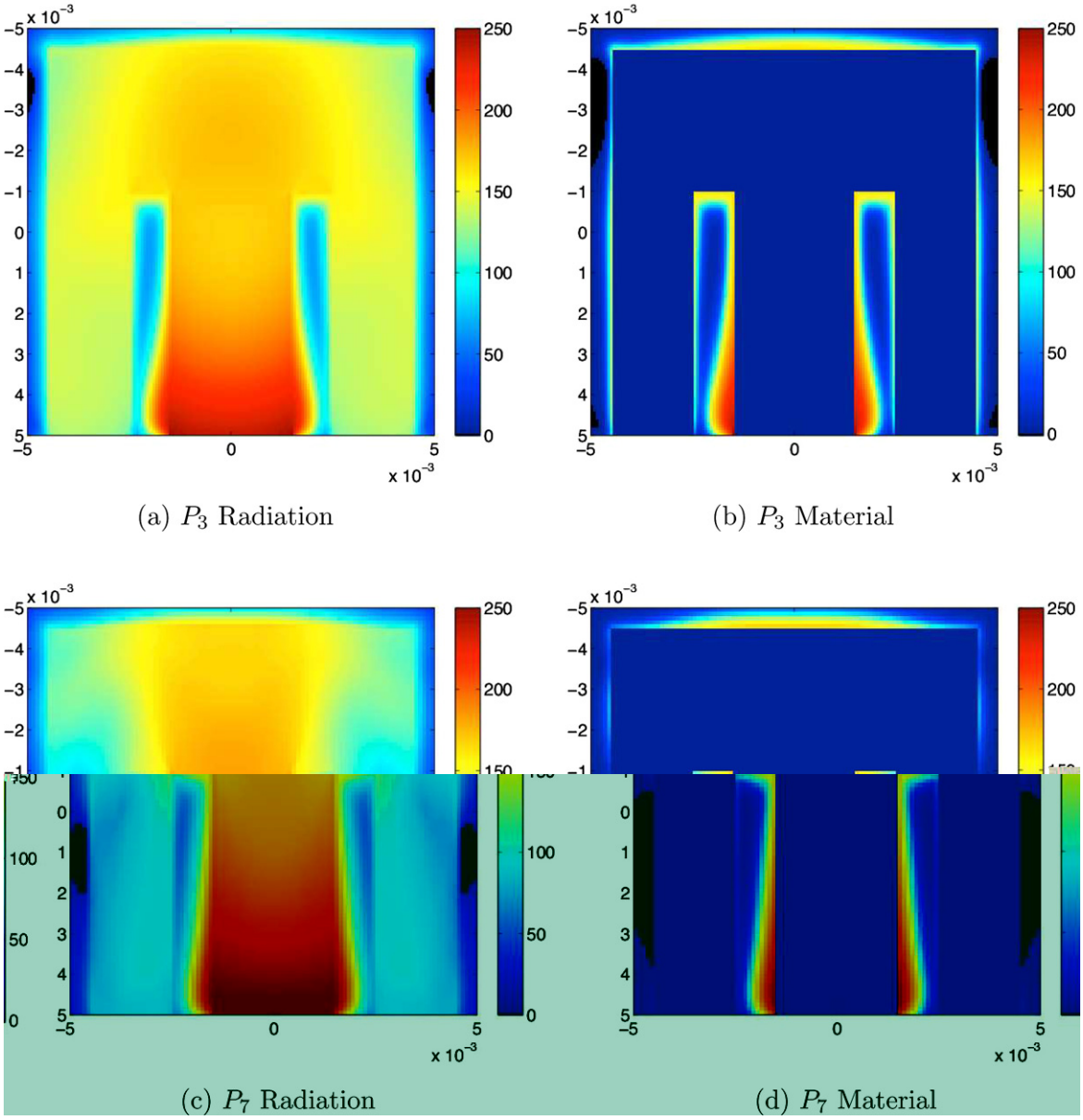

Fig. 12. Radiation and material temperature (eV) at 6 ns for the thermal duct problem from P_3 and P_7.

ditioners (either algebraic or physics-based such as a diffusion synthetic preconditioner) could reduce the number of GMRES iterations by a factor of 2 or 3 (a reasonable reduction), the implicit method would perform markedly better than an explicit method.

8. Conclusions

We have demonstrated important aspects of the P_n approximation for solving thermal radiative transfer problems. In the free-streaming limit we proved that for any finite order of expansion the P_n equations can give solutions with a negative energy density. We also developed a numerical method to solve the P_n equations in order to examine how the approximation behaves in more complicated situations.

For the Su–Olson benchmark problem we were able to study the convergence of P_n to transport in the one-dimensional case. Results showed that P_1 is a poor approximation for this problem, however, increasing the order of approximation beyond P_3 demonstrated approximately linear convergence in n. The P_7 solution captured the transport solution well.

In two-dimensional problems our results had negative energy densities as predicted by our theorem. The negative energy densities persisted even at long times. Increasing the order of the P_n expansion decreased the magnitude of the largest negative density, however, increasing n did in some cases lead to a larger area of negative energy density in the solution. These results also showed that the material temperature can become negative, a result outside the scope of the theorem.

The negative energy densities are not necessarily a mortal blow to the possibility of using the P_n equations for production purposes. There are ad hoc ways of dealing with quantities becoming unphysically negative in large code projects. These can take the form of a temperature floor that does not allow the material temperature to become negative. It has yet to be determined if such a floor would cause problems in a coupled simulation using the P_n method. This option, while destroying energy conservation, would not affect the negative radiation energy densities in vacuum regions.

While there cannot be a guarantee of positivity for solutions of the standard P_n equations for a finite expansion order n, for many problems there will be an order of expansion that reduces the negatives to a negligible amount. Some important future work would be to understand how these negatives go away as the order of the expansion is increased. For example, in the thermal duct problem will P_{15} reduce the negatives to an acceptable amount? At this point little is known theoretically about the magnitude of negative energy density values in the P_n equations as n is increased.

The numerical method we used in this study was an implicit upwind discretization of the P_n equations. Implicit time integration is important because the radiation propagation time scale is much shorter than the material energy time scale. Our implicit approach solved the fully coupled, nonlinear radiation-material energy equations. With the implicit method we were able to solve thermal radiation transport problems on the time scale of the material energy equation rather than on a time scale limited by the CFL limit. These results represent the first use of an implicit Riemann method for thermal radiation transport.

We successfully modified our previous quasi-linear approach to thermal transport problems. An implicit method for a high-resolution spatial scheme requires the solution of a system of nonlinear equations at each time step. We were able to reduce the computational cost of solving these equations by using a two-step approach that is quasi-linear in the radiation transport terms. The quasi-linear approach was developed out of the fact that the underlying P_n equations are linear in the radiation streaming and that the nonlinearities in streaming were added to get a high-resolution spatial scheme.

An approximate comparison of the performance of our implicit method and an explicit method shows that our unaccelerated method is about as efficient as an explicit method for one of the problems we solved. We expect that future investigations into the acceleration of our method will make the implicit method more efficient. We also found that as the CFL number increases, the number of GMRES iterations remains stable. This result means that as the mesh is refined, the implicit method will perform better than an explicit method.

While our and others' results show that there is still important work to be done in the realms of numerics and analysis of the P_n equations, these methods still show promise. P_n methods are at sizeable disadvantage to S_n methods because the latter has such a large body of research regarding analysis and implementation.

Acknowledgments

R.G.M. would like to thank T.J. Urbatsch for his helpful comments on a draft version of this article. The authors would also like to thank the anonymous referees for their insightful comments.

References

[1] E.E. Lewis, W.F. Miller, Computational Methods of Neutron Transport, John Wiley and Sons, 1984.
[2] K.A. Mathews, On the propagation of rays in discrete ordinates, Nucl. Sci. Eng. 132 (1999) 155.
[3] R.G. McClarren, J.P. Hollway, T.A. Brunner, Analytic P_1 solutions for time-dependent, thermal radiative transfer in several geometries, J. Quant. Spectrosc. Radiat. Transfer 109 (2008) 389–403.

[4] T.A. Brunner, J.P. Holloway, Two dimensional time dependent Riemann solvers for neutron transport, J. Comput. Phys. 210 (1) (2005) 386–399.
[5] T.A. Brunner, J.P. Holloway, One-dimensional Riemann solvers and the maximum entropy closure, J. Quant. Spectrosc. Radiat. Transfer 69 (2001) 543–566.
[6] R.G. McClarren, J.P. Holloway, T.A. Brunner, T.A. Mehlhorn, A quasi-linear implicit Riemann solver for the time-dependent P_n equations, Nucl. Sci. Eng. 155 (2007) 290–299.
[7] R.G. McClarren, Spherical Harmonics Methods for Thermal Radiation Transport, Ph.D. Thesis, University of Michigan, Ann Arbor, Michigan, 2007.
[8] G.C. Pomraning, The Equations of Radiation Hydrodynamics, Pergamon Press, Oxford, 1973.
[9] J.E. Morel, T.A. Wareing, R.B. Lowrie, D.K. Parsons, Analysis of ray-effect mitigation techniques, Nucl. Sci. Eng. 144 (2003) 1–22.
[10] T.A. Brunner, Riemann Solvers for Time-dependent Transport based on the Maximum Entropy and Spherical Harmonics Closures, Ph.D. Thesis, University of Michigan, Ann Arbor, Michigan, 2000.
[11] G.C. Pomraning, A generalized P–N approximation for neutron transport problems, Nukleonik 6 (1964) 348–356.
[12] D.A. Knoll, W.J. Rider, G.L. Olson, An efficient nonlinear solution method for non-equilibrium radiation diffusion, J. Quant. Spectrosc. Radiat. Transfer 63 (1999) 15–29.
[13] R.J. Leveque, Numerical Methods for Conservation Laws, Birkhäuser Verlag, Boston, USA, 1992.
[14] B. van Leer, Towards the ultimate conservative difference scheme. II. Monotonicity and conservation combined in a second-order scheme, J. Comput. Phys. 14 (1974) 361–370.
[15] R. McClarren, J.P. Holloway, T.A. Brunner, Establishing an asymptotic diffusion limit for Riemann solvers on the time-dependent P_n equations, in: International Topical Meeting on Mathematics and Computation, Supercomputing, Reactor Physics and Nuclear and Biological Applications, American Nuclear Society, Avignon, France, 2005.
[16] R.B. Lowrie, J.E. Morel, Issues with high-resolution Godunov methods for radiation hydrodynamics, J. Quant. Spectrosc. Radiat. Transfer 69 (2001) 475–489.
[17] C.T. Kelley, Iterative Methods for Linear and Nonlinear Equations Frontiers in Applied Mathematics, Society for Industrial and Applied Mathematics, Philadelphia, USA, 1995.
[18] G. Hedstrom, Models of difference schemes for $u_t + u_x = 0$ by partial differential equations, J. Comput. Phys. 29 (1975) 969–977.
[19] M. Heroux, R. Bartlett, V.H.R. Hoekstra, J. Hu, T. Kolda, R. Lehoucq, K. Long, R. Pawlowski, E. Phipps, A. Salinger, H. Thornquist, R. Tuminaro, J. Willenbring, A. Williams, An Overview of Trilinos, Technical Report SAND2003-2927, Sandia National Laboratories, 2003.
[20] B. Su, G.L. Olson, An analytic benchmark for non-equilibrium radiative transfer in an isotropically scattering medium, Ann. Nucl. Energy 24 (13) (1997) 1035–1055.
[21] G.L. Olson, L.H. Auer, M.L. Hall, Diffusion, P_1, and other approximate forms of radiation transport, J. Quant. Spectrosc. Radiat. Transfer 64 (2000) 619–634.